Global two-fluid simulations of geodesic acoustic modes in strongly shaped tight aspect ratio tokamak plasmas
J. R. Robinson, B. Hnat, A. Thyagaraja, K. G. McClements, P. J. Knight et al.
Phys. Plasmas 20, 052302 (2013)

AIP | Physics of Plasmas

Global two-fluid simulations of geodesic acoustic modes in strongly shaped tight aspect ratio tokamak plasmas

J. R. Robinson, B. Hnat, A. Thyagaraja, K. G. McClements, P. J. Knight et al.

Citation: Phys. Plasmas **20**, 052302 (2013); doi: 10.1063/1.4804271
View online: http://dx.doi.org/10.1063/1.4804271
View Table of Contents: http://pop.aip.org/resource/1/PHPAEN/v20/i5
Published by the American Institute of Physics.

Global two-fluid simulations of geodesic acoustic modes in strongly shaped tight aspect ratio tokamak plasmas

J. R. Robinson,[1,a)] B. Hnat,[1] A. Thyagaraja,[2] K. G. McClements,[3] P. J. Knight,[3] A. Kirk,[3] and MAST Team[3]
[1]*Physics Department, University of Warwick, Coventry, CV4 7AL, United Kingdom*
[2]*H.H. Wills Physics Laboratory, University of Bristol, Bristol BS8 1TL, United Kingdom*
[3]*EURATOM/CCFE Fusion Association, Culham Science Centre, Abingdon, OX14 3DB, United Kingdom*

(Received 21 January 2013; accepted 8 April 2013; published online 7 May 2013)

Following recent observations suggesting the presence of the geodesic acoustic mode (GAM) in ohmically heated discharges in the Mega Amp Spherical Tokamak (MAST) [J. R. Robinson *et al.*, Plasma Phys. Controlled Fusion **54**, 105007 (2012)], the behaviour of the GAM is studied numerically using the two fluid, global code CENTORI [P. J. Knight *et al.* Comput. Phys. Commun. **183**, 2346 (2012)]. We examine mode localisation and effects of magnetic geometry, given by aspect ratio, elongation, and safety factor, on the observed frequency of the mode. An excellent agreement between simulations and experimental data is found for simulation plasma parameters matched to those of MAST. Increasing aspect ratio yields good agreement between the GAM frequency found in the simulations and an analytical result obtained for elongated large aspect ratio plasmas. © *2013 AIP Publishing LLC*. [http://dx.doi.org/10.1063/1.4804271]

I. INTRODUCTION

Magnetically confined plasmas are out-of-equilibrium, driven systems which show strongly nonlinear behaviour. This nonlinear dynamics leads to energy transfer between diverse range of scales. It is well established that micro-scale instabilities, with most unstable modes in the range of 10–30 gyro radii, extract the energy from the local gradients in density and temperature and convert it turbulent flows. Upon achieving certain amplitude, these turbulent fluctuations can drive large scale flows, either via the inverse cascade or, for example, via modulation instability four wave interactions. The large scale flows, which emerge from this dynamics have been termed Zonal Flows (ZFs). Analytical and numerical works confirmed the development of these flows in realistic plasma conditions and this led to a dramatic shift in our understanding of the energy channels in turbulent fusion plasma. It is now widely recognized that, despite being linearly stable, zonal flows can regulate the level of plasma fluctuations by extracting the energy from turbulence and by enhancing dissipation via eddy shearing mechanism. Recently, the effect of resonant magnetic perturbations (RMPs) on this acoustic mode was studied on Mega Amp Spherical Tokamak (MAST) and the results strongly suggest that RMPs suppress geodesic acoustic mode (GAM) and this leads to increase level of turbulence.[1] Since RMPs may play a vital role in suppressing large edge localized modes (ELMs) on future fusion reactors, such as ITER, the understanding of GAM is paramount to the further progress of controlled fusion.

Zonal flows are radially localised ($k_r \neq 0$) axisymmetric and poloidally symmetric ($m = n = 0$, where m and n are the poloidal and toroidal mode numbers, respectively) electrostatic potential modes, with frequency $\Omega \approx 0$. GAMs[2] results from the compressibility of the zonal flows in toroidal geometry where a coupling to an acoustic mode with $m = \pm 1$ is due to the geodesic curvature of the confining magnetic field. GAMs have been identified in many devices[3–5] as well as numerical simulations.[6] The non-zero frequency characteristic of the GAM is especially useful for experimental observations relating turbulence and zonal flow phenomena, where the exact poloidal structure of the mode may not be accessible. In this context, numerical studies of GAM, especially the functional dependence of its dispersion relation on plasma characteristic and confinement geometry is of great interest. While analytical work predicts the dispersion relation for the GAM in the case of circular cross-section and large aspect ratio[7–11] and finite aspect elliptical cross-section,[12,13] experimental observations demonstrate the departure from this formula for realistic shaping.[14] To the best of our knowledge, no studies directly comparing experiment to simulations of this kind have been performed for spherical tokamaks to date.

In this paper, we investigate the characteristic of GAMs in MAST-like Ohmic plasmas. We use the CENTORI[15] global two fluid simulation code, which allows us to explore the effects of varying the shape of the poloidal plasma cross-section in addition to other key plasma parameters. We will report the effect of the finite aspect ratio, elongation, safety factor, and the ion-electron temperature ratio on the observed GAM frequency.

II. CENTORI

CENTORI is a new toroidal two-fluid electromagnetic turbulence code that can evolve the equilibrium with an arbitrary aspect ratio and high plasma beta. The magnetic configuration is set by specifying the axis position, toroidal field, plasma current and poloidal field coil positions and currents, together with density and temperature profiles, and other

a)Electronic mail: james.robinson@warwick.ac.uk

initial conditions. Thus, it is relatively simple to match magnetic equilibrium reconstructions (EFIT) of experimental discharges in MAST, and other tokamaks. From the cylindrical (R, Z, ζ) coordinate system of the equilibrium solver, the simulation space is defined on a dimensionless (ψ, θ, ζ) grid, such that the Jacobian is constant on a flux surface, with $\psi^{1/2}$ proportional to the normalized radius. The system of equations co-evolves the equilibrium quantities, and fluctuating parts of $\tilde{n}_e, \tilde{T}_e, \tilde{T}_i, \tilde{\mathbf{v}}_i, \tilde{\mathbf{J}}, \tilde{A}_\zeta$, incorporating neoclassical diffusivities, Ware pinch, and parallel ion relaxation terms. For full details, we refer the reader to Ref. 15.

The simulations were set up on a grid of $128 \times 128 \times 32$ radial, poloidal, and toroidal points, respectively, with a timestep of 0.5 ns to satisfy the Courant conditions. Evolution of the equilibrium, and output was performed every 5000 timesteps, giving a temporal resolution of 200 kHz, matching that of the reciprocating probe used in the MAST experiments. All simulations were run for at least 1 ms or until approximately steady state conditions were reached, before using the data for further analysis.

III. MATCHING MAST OHMIC DISCHARGE

A simulation was set up to match the conditions of MAST discharge 21856, in which GAMs were observed at 10 kHz. Figure 1 shows the EFIT reconstruction of the MAST equilibria overlaid with contours from the simulation showing good agreement with the overall position and shaping. Panels (b) and (c) of the figure show the corresponding density and temperature from a Thomson scattering measurement taken during the middle of the MAST discharge ($t = 0.35$ s) compared to the simulation. The value of n_e, T_e, and T_i are fixed at the plasma edge as per the CENTORI boundary conditions,[15] motivated by the experimental values. The edge density and temperature gradients can be seen to reach equilibrium values fairly close to experimental values. However, the values in the core differ quite significantly, possibly due to insufficient radial resolution close to the axis. We performed several simulations with varying background diffusivities to verify that the discrepancy in the core does not affect the behavior in the edge.

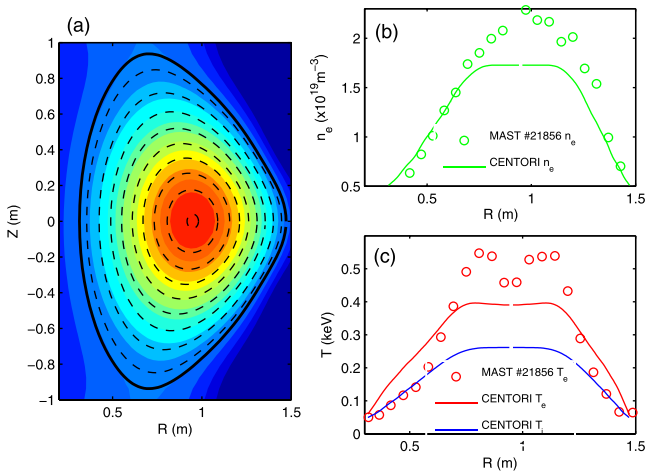

FIG. 1. (a) EFIT reconstruction of MAST discharge 21856 (filled contours) vs CENTORI simulation equilibrium flux surfaces (black lines). (b) Midplane density profile from Thomson scattering measurements (open circles) and CENTORI simulation (solid curve, (c) Midplane Thomson scattering electron temperature profile (open circles), simulation T_e (red curve), and T_i (blue curve).

IV. MODE STRUCTURE

A strong electrostatic mode spontaneously develops from the random seed variations with $m = n = 0$ in potential and an up/down asymmetric m = 1 dominant component in the density fluctuations. In the highly shaped plasma residual $m > 1$, density fluctuations reach the inboard and outboard midplane. Figure 2 shows a snapshot of the normalized potential and density fluctuations of the fully developed mode. The growth and saturation of the mode over the first millisecond of the simulation can be seen in Figure 3(a) after which time the density fluctuations remain roughly constant with an outward propagating phase. The radial structure and propagation is illustrated in Fig. 3(b), showing a series of profiles at $\Delta t = 10\mu$s intervals forming the radial envelope of the mode. The mean density fluctuation level varies around the poloidal cross-section with a slight asymmetry between top and bottom as shown in Figure 3(c), which also shows a $\tilde{n}/\langle n \rangle \sim 3\%$ level of fluctuations propagating to the outboard midplane, and up to 8% on the inboard side, but peaking at a slightly smaller radius.

Floating potential measurements were obtained via reciprocating probe, at a single location 4 cm inside the last closed flux surface, on the outboard midplane, over a 3 ms time interval, with a sampling rate of 400 kHz, in MAST discharge 21856. Numerical data were obtained from a CENTORI simulation of this discharge, for the same spatial location (the average potential of two radial grid cells was used) and with the same sampling rate. The resultant power spectra are plotted in Figure 4. Minimal smoothing was also applied to both power spectra to reduce the noise in order to bring out the features of interest. The simulation and experiment show remarkable agreement in slope, both on the low and high frequency of the GAM peak, and in magnitude. The radial wavelength varies over the width of the mode, so the

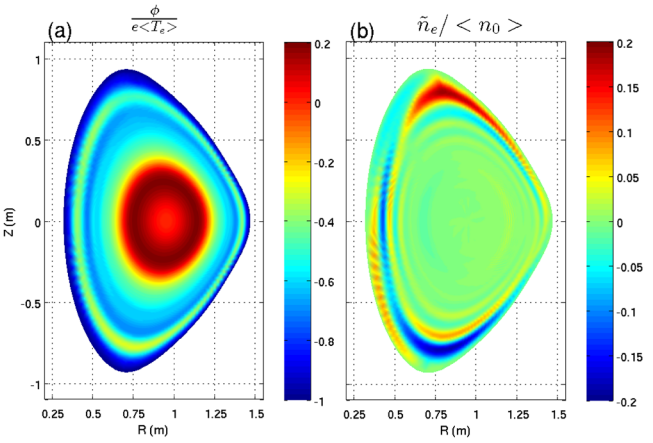

FIG. 2. Snaphsot at $t = 2.58$ ms of (a) potential, normalised to flux surface average electron temperature, showing dominantly m = 0 structure, and (b) density fluctuation, normalised to the flux surface average over 1 ms, showing mainly m = 1 up/down mode, but with significant deviation due to shaping.

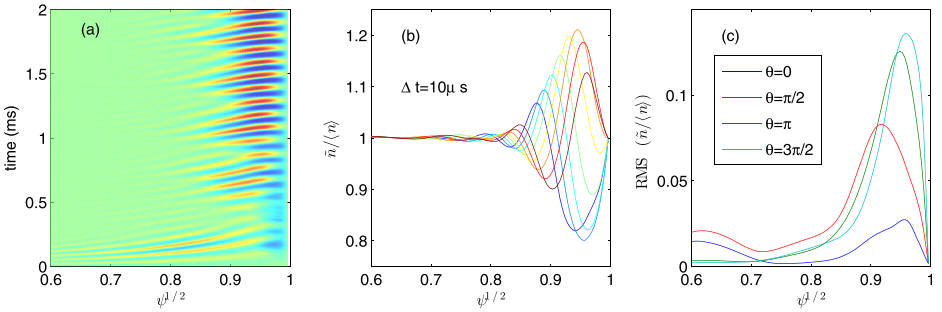

FIG. 3. (a) Time evolution of density fluctuations with radius along $\theta = \pi/2$ for the first 2 ms of simulation (b) Series of snapshots of density fluctuation at 10 μs intervals showing envelope and outward phase propagation (c) Root-mean-square of density fluctuations for t = 2–5 ms at different poloidal coordinates.

wavenumber more easily determined by tracking the phase velocity of each fluctuation peak in turn as it propagates outwards along the $\theta = \pi/2$ contour over the time window $t = 2$–5 ms as show in Figure 5(a). The wavenumber is then found from the relation $v_p = \omega/k$, with the assumption that the dominant frequency is constant over the width of the plateau. The radial phase velocity is seen to rise from $\approx$1.5 km/s at a normalised radius of $\psi^{1/2} = 0.86$ to $\approx$3.0 km/s at $\psi^{1/2} = 0.92$, before dropping back towards the edge. The wavelength corresponding to $\hat{k} = 0.05 - 0.1$ is in the range of 15–30 cm towards the X-points.

V. THEORETICAL GAM SHAPING FACTORS

While there have been many studies of the GAM under idealized large aspect ratio, circular,[7,9–11] and elliptical[17,18] cross section conditions, in which useful insights can be made on the growth, damping mechanisms, and dispersion relations, the extension to tight aspect ratios and realistic shaping parameters is more difficult. From a collisionless gyro-kinetic approach, using the ratio of the magnetic drift frequency $\omega_D = k|\nabla r|\hat{\mathbf{x}} \cdot \mathbf{b} \times (\mu \nabla B + m v_\parallel^2 \mathbf{b} \cdot \nabla \mathbf{b})/m\Omega$ to the poloidal transit frequency $\omega_t = v_\parallel B_p/[(dl/d\theta)B]$. The limiting cases of large orbit drift width (ODW) $\omega_D \gg \omega_t$ Ref. 12 extends the model of Ref. 11, and small ODW $\omega_D \ll \omega_t$ (Ref. 13) based on[8,16] solve the linear gyrokinetic equation in terms of inverse aspect ratio ϵ, elongation κ, Shafranov shift gradient Δ', safety factor q, and temperature ratio $\tau = T_e/T_i$. The gradient of the elongation also appears as $s_\kappa = (r/\kappa)\partial_r \kappa \approx (\kappa - 1)/\kappa$. Triangular deformation of the plasma cross section is not taken into account in the ODW model.

Using the small ODW limit, appropriate for the MAST edge conditions, of Ref. 13, but neglecting the small corrections due to Shafranov shift gradient, the GAM frequency is given by

$$\frac{\omega_{\mathrm{GAM}}}{v_{T_i}/R_0} = \sqrt{\left(\frac{7}{4}+\tau\right)\left(\frac{2}{\kappa^2+1}\right)\left(1-\frac{s_\kappa}{2}\frac{7+2\tau}{7+4\tau}\right)} \times \left(1-\epsilon^2\frac{9\kappa^2+3}{8\kappa^2+8}\right) \times \left[1+\frac{\kappa^2+1}{4q^2}\left(\frac{23}{8}+2\tau+\frac{\tau^2}{2}\right)\left(\frac{7}{4}+\tau\right)^{-2}\right]. \quad (1)$$

The growth rate of the mode is also given by the theory, but here we will concentrate on the mode frequency. The large ODW limit gives a similar form for the frequency that yields only a few percent difference, but has a different growth rate, as detailed in Ref. 13. The 7/4 ion adiabatic coefficient appearing in collisionless gyro-kinetic models, and recovered in fluid models if one retains anisotropic pressure terms,

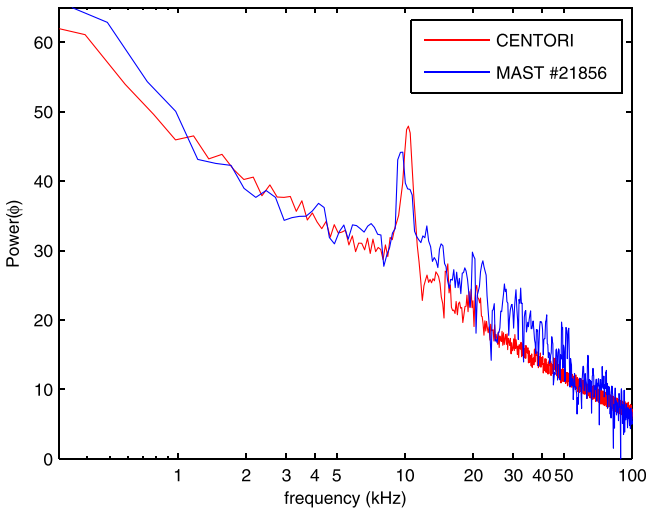

FIG. 4. Power spectra of experimental and simulated potential fluctuations $\tilde{\phi}$, normalized to the standard deviation of the fluctuations over the time period, on the outboard midplane 4 cm inside the last closed flux surface.

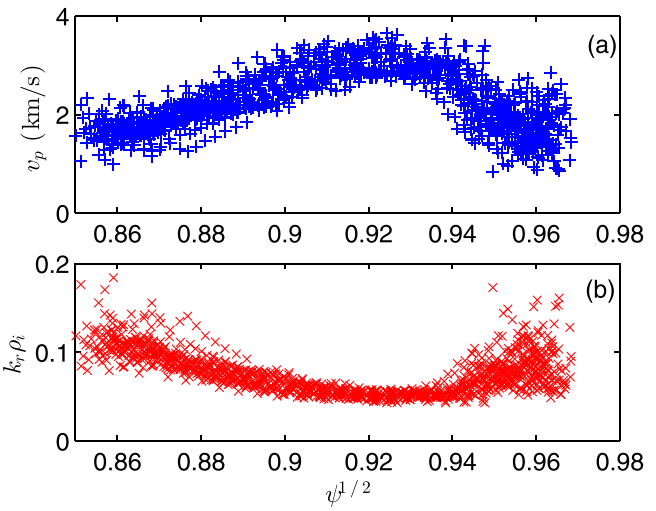

FIG. 5. (a) Radial (outward) phase velocity of peaks in density fluctuation, (b) normalized radial wavenumber $\hat{k} = k_r\rho_i$, where $k_r = \omega_{\mathrm{GAM}}/v_p$.

is not expected to be recovered by CENTORI, Eq. (1) is chosen to illustrate a form of the relationship due to shaping. Although recently it has been shown,[19] the gyro-kinetic $(7/4+\tau)$ term reduces to the isotropic fluid-like $(1+\tau)$ in high collisionality.

VI. VARIATION WITH R_0

In order to test the agreement of the analytical shaping factor in Eq. (1) with simulation, a series of runs were performed keeping all the key parameters the same ($B_0 = 0.5\,\mathrm{T}$ and $I_p = 0.5\,\mathrm{MA}$), except moving the major radius R_0, of the magnetic axis, from the MAST configuration of 95 cm inwards to 85 cm, and outwards to 110, 120, and 150 cm. The poloidal and divertor field coils were also moved out to keep the overall shaping broadly similar, but with the plasma relaxing to find its own equilibrium, giving an elongation reducing from 1.85 to 1.43, and safety factor at the position of the peak GAM reducing from $q = 7.96$ in the very tight 85 cm case to $q = 2.87$ at 150 cm. A GAM-like mode was observed in all cases with the frequency only reducing from 10.6 kHz at $R_0 = 85\,\mathrm{cm}$ to 7.98 kHz at $R_0 = 150\,\mathrm{cm}$ despite the approximately constant temperatures and $1/R_0$ dependence of the large aspect approximation. Taking the constant $\theta = \pi/2$ radial contour, a Fourier transform was taken over a 3 ms window, once the simulation had reached approximately steady state conditions at each position. The radial frequency plateaux, observed experimentally in ASDEX Upgrade,[14] can be seen in the density fluctuations as shown in Figure 6, where the colour scale is $\log(|\tilde{n}_e/n_0|^2)$. Overlaid are lines for the sound transit frequency $c_s/2\pi R_0$ and the predicted local GAM frequency.

The series of plateaux can be seen to extend deeper into the core of the smaller radius plasmas. Interpreting Figure 6, the mode at each excited frequency appears to propagate outwards until that frequency approaches the local sound transit frequency where it is damped. So for the cases where the region between the lines is large, the mode can exist as

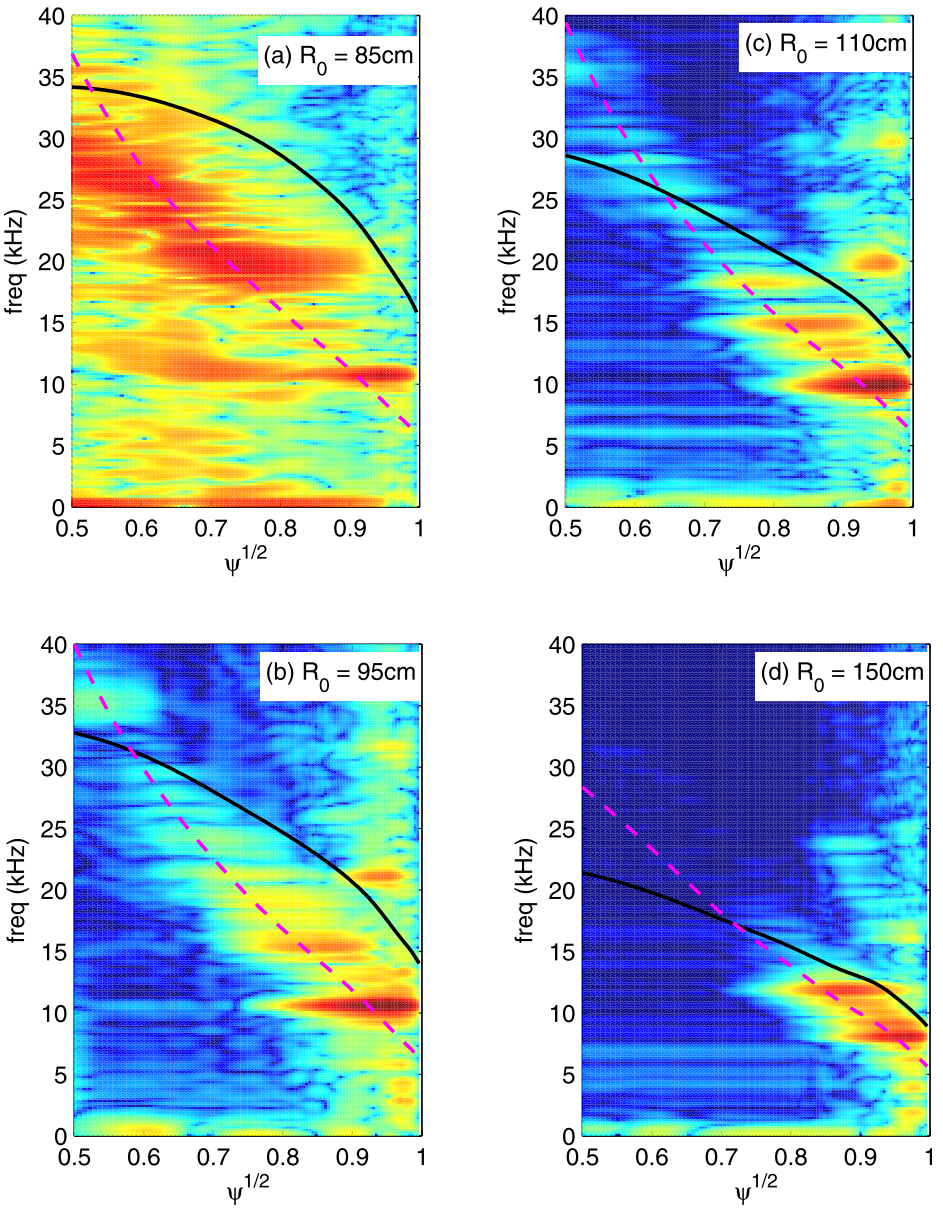

FIG. 6. Density fluctuation power for (a) $R_0 = 85\,\mathrm{cm}$, (b) $R_0 = 95\,\mathrm{cm}$, (c) $R_0 = 110\,\mathrm{cm}$, and (d) $R_0 = 150\,\mathrm{cm}$. Black line shows the sound speed transit frequency $f_{c_s} = c_s/(2\pi R_0)$, the magenta dashed line is the predicted local GAM frequency from Eq. (1).

multiple overlapping plateaux. The position of the main (outer) GAM peak can also be seen to be pushed out slightly in the large R_0 (low q) case going from normalized radius $\psi^{1/2} = 0.935$ to $\psi^{1/2} = 0.956$. Also, the relative amplitude of the second plateau grows with respect to the outer mode, so by $R_0 = 1.5$ m, they are on a par with each other. It should be noted that due to numerical limitations, the simulation region cannot extend fully to the X-points and so the grid boundary is at 95% of the equilibrium flux at the last closed flux surface.

VII. DISCUSSION

The two-fluid simulations show strong $m = n = 0$ potential and $m = 1$, $n = 0$ density fluctuations of a GAM with the frequency showing remarkable agreement with the experimental measurements in MAST,[1] confirming the observed mode as a GAM. Also the simulations show in the highly shaped configuration of MAST that although the $m = 1$ up/down nature of the density fluctuations is dominant, one can expect a small, but experimentally measurable, perturbation at the outboard midplane, as was seen.

Many features of the simulation match previous observations in other tokamaks, such as the overlapping plateaux,[14] manifesting as the peak splitting in two at certain radial locations. The radial extend of each plateau envelope is around one wavelength. The variation of radial wavelength around the poloidal section is most easily seen in the potential (see Figure 2(a)), following the flux surfaces getting longer towards the X-points. Combining this with the variation in Larmor radius gives a variation in $k_r \rho_i$ from 0.01 to 0.2.

We compare the value of the frequency at the centroid of the main and second plateaux from each simulation with the analytical model by inserting the local values q, κ, ϵ, and τ into Eq. (1), shown in Figure 7, where the horizontal error bars of ± 500 Hz correspond to the Fourier transform resolution, and the vertical error bars represent the sensitivity of the analytical prediction to a variation of $\pm 20\%$ in τ. Taking all the results over the wide variety of parameters the simulations show a strong linear relationship, ($R^2 = 0.966$) with the ODW model as expressed by Eq. (1), but underestimating the GAM frequency by 12%. This is evident from Figures 6(a)–6(d), where the predicted frequency (magenta dashed lines) coincides with the inner edge of the plateaux rather than the points where they reach maximum amplitude.

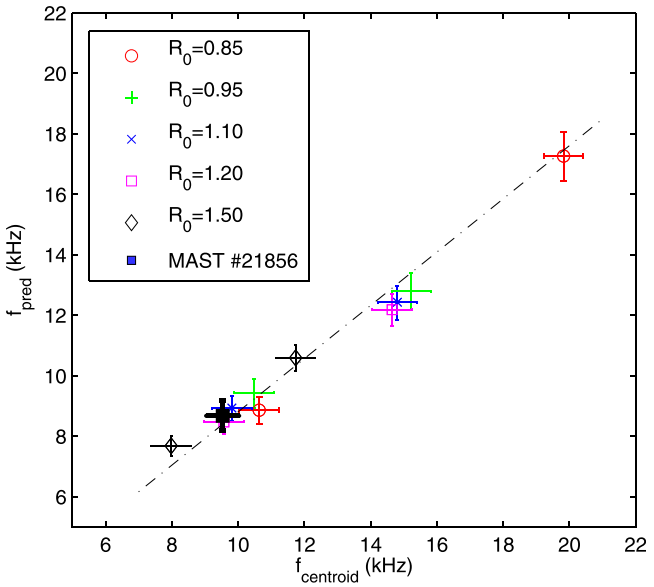

FIG. 7. Simulation vs predicted GAM frequency for main and secondary plateaux. Linear fit: gradient = 0.88 ± 0.12, $R^2 = 0.966$, together with MAST discharge 21856 GAM peak.

VIII. CONCLUSIONS

In summary, we have reported spontaneous excitation of the geodesic acoustic mode in two-fluid simulations of MAST-like ohmic L-mode plasmas. The simulations match in frequency both experimental observations in MAST and theoretical predictions for the mode in elongated plasmas for a range of geometries. This also provides a strong benchmark test of the electrostatic behaviour of the code.

The importance of the GAM in relation to zonal flows and as a benign sink for turbulent energy suggests this needs to be investigated further. So, while this work that has concentrated on the frequency, location, and structure of the mode, future work is planned to quantify the growth, saturation level, and damping of the mode, with particular attention on the edge rotation induced by resonant magnetic perturbations. Such studies should be performed not only for the relatively cool ohmic, spherical tokamak plasmas considered here but also for the higher temperature, auxiliary-heated conditions in which L-H transitions can occur, in both JET and ITER.

ACKNOWLEDGMENTS

The Warwick team acknowledges EPSRC support (Grant No. EP/G02748X/1). This work was part-funded by the RCUK Energy Programme under Grant No. EP/I501045 and the European Communities under the contract of Association between EURATOM and CCFE. The views and opinions expressed herein do not necessarily reflect those of the European Commission.

[1]J. R. Robinson, B. Hnat *et al.*, Plasma Phys. Controlled Fusion **54**, 105007 (2012).
[2]N. Winsor, J. L. Johnson, and J. M. Dawson, Phys. Fluids **11**, 2448 (1968).
[3]M. Jakubowski, R. J. Fonck, and G. R. McKee, Phys. Rev. Lett. **89**, 265003 (2002).
[4]G. D. Conway, B. Scott, J. Schirmer, M. Reich, A. Kendl, and ASDEX Upgrade Team, Plasma Phys. Controlled Fusion **47**(8), 1165 (2005).
[5]Y. Hamada, A. Nishizawa, T. Ido, T. Watari, M. Kojima, Y. Kawasumi, K. Narihara, K. Toi, and JIPPT-IIU Group, Nucl. Fusion **45**(2), 81 (2005).
[6]S. V. Novakovskii, C. S. Liu, R. Z. Sagdeev, and M. N. Rosenbluth, Phys. Plasmas **4**(12), 4272 (1997).
[7]A. I. Smolyakov, C. Nguyen, and X. Garbet, Plasma Phys. Controlled Fusion **50**, 115008 (2008).
[8]Z. Gao, K. Itoh, H. Sanuki, and J. Q. Dong, Phys. Plasmas **13**, 100702 (2006).
[9]V. P. Lakhin, V. I. Ilgisonis, and A. I. Smolyakov, Phys. Lett. A **374**, 4872 (2010).
[10]A. G. Elfimov, R. M. O. Galvão, and R. J. F. Sgalla, Plasma Phys. Controlled Fusion **53**, 105003 (2011).
[11]Z. Qiu, L. Chen, and F. Zonca, Plasma Phys. Controlled Fusion **51**, 012001 (2009).

[12]Z. Gao, Phys. Plasmas **17**, 092503 (2010).
[13]Z. Gao, Plasma Sci. Technol. **13**, 15 (2011).
[14]G. D. Conway *et al*., Plasma Phys. Controlled Fusion **50**, 055009 (2008).
[15]P. J. Knight *et al*., Comput. Phys. Commun. **183**, 2346 (2012).
[16]Z. Gao, K. Itoh, H. Sanuki, and J. Q. Dong, Phys. Plasmas **15**, 072511 (2008).
[17]Z. Gao, L. Peng, P. Wang, J. Dong, and H. Sanuki, Nucl. Fusion **49**, 045014 (2009).
[18]P. Angelino, X. Garbet, L. Villard, A. Bottino, A. Jolliet *et al*., Phys. Plasmas **15**, 062306 (2008).
[19]Z. Gao, Phys. Plasmas **20**, 032501 (2013).